

Chaos Pass Filter: Linear Response of Synchronized Chaotic Systems

Wolfgang Kinzel,¹ Johannes Kestler,¹ and Ido Kanter²

¹*Institute for Theoretical Physics, University of Würzburg, Am Hubland, 97074 Würzburg, Germany*

²*Minerva Center and the Department of Physics, Bar-Ilan University, Ramat-Gan, 52900 Israel*

(Dated: May 21, 2008)

The linear response of synchronized chaotic units with delayed couplings and feedback to small external perturbations is investigated in the context of communication with chaos synchronization. For iterated chaotic maps, the distribution of distances is calculated numerically and, for some special cases, analytically as well. Depending on model parameters, this distribution has power law tails leading to diverging moments of distances in the region of synchronization. The corresponding linear equations have multiplicative and additive noise due to perturbations and chaos. The response to small harmonic perturbations shows resonances related to coupling and feedback delay times. For perturbation from a binary message the bit error rate is calculated. The bit error rate is not related to the transverse Lyapunov exponents, and it can be reduced when additional noise is added to the transmitted signal. For some special cases, the bit error rate as a function of coupling strength has the structure of a devil's staircase, related to an iterated function system. Finally, the security of communication is discussed by comparing uni- and bi-directional couplings.

I. INTRODUCTION

Chaotic systems which are coupled to each other, can synchronize to a common chaotic trajectory [1–3]. Even if dynamic systems exchange signals with a large delay time they still can synchronize completely, without any time shift [4–7]. This phenomenon is presently attracting a lot of attention, partly because of its counter-intuitive fundamental aspect of nonlinear dynamics, and partly because of its potential for secure communication with chaotic signals [8–10], for a review see [11]. In fact, broadband communication with synchronized chaotic semiconductor lasers has recently been demonstrated over 120 km in a public fiber network [12].

There are several ways to transmit a message with chaotic signals. One of them depends on a phenomenon which has been coined “chaos pass filter” [13, 14]. It was observed that a chaotic system which is driven by the chaotic trajectory of its partner plus the (small) message responds essentially only with the trajectory but not with the message. Thus the chaotic system filters out any perturbation and responds with its chaotic trajectory. Using this mechanism, the receiving unit can recover the message just by subtracting the incoming signal from its own variables.

Adding a small message to a chaotic carrier has the potential for chaotic communication [11]. Obviously, it is difficult to extract the message from the irregular trajectory of the transmitted signal. However, when an adversary has access to the signal, and when he knows all the details including the parameters of the sending unit, he may be able to use an identical unit, synchronize it as well and extract the message. Recently, it has been suggested that even in this case secret communication may be possible. Two chaotic units which interact by bidirectional transmission have an advantage over an attacker driven by a unidirectional signal. This difference between bi- and unidirectional transmission opens applications on public cryptography [15][16][17].

Chaos pass filter is observed in experiments on electronic circuits and lasers and in simulations of chaotic systems. But it is not well understood. When chaotic units synchronize, their chaotic trajectories will be attracted by a synchronization manifold. Any perturbation of one of the two trajectories has two effects: Parallel to the synchronized manifold the perturbation will explode, since the system is chaotic. But perpendicular to the manifold the perturbation will decay to zero, thus the system will synchronize again. However, this does not necessarily mean that a permanent perturbation like a secret message is damped by the chaotic receiver.

The linear response of chaotic systems to an external perturbation has been investigated before, mainly in the context of linear stochastic systems with multiplicative and additive noise [18, 19]. In this paper the linear response of synchronized chaotic units is investigated. To obtain analytic results, we use iterated maps to study chaos pass filter, but many of the results are also observed in numerical simulations of chaotic differential equations. In section II, the models are introduced and the linearized equations for the perturbations are derived. In section III, we define quantities which measure the linear response to noisy signals. We observe large excursions off the synchronization manifold which lead to a continuum of diverging moments. We calculate resonances, bit error rates, devil's stair cases and Lyapunov spectra. In section IV, a third unit, an attacker, is considered which is driven by the exchanged signal and tries to synchronize with the communicating partners. The last section summarizes and discusses our results.

II. THE MODELS

Consider two chaotic units A and B which are coupled to each other by a function of their internal variables. The exchanged signal arrives at the partner with some delay time τ . Since we want to compare our results

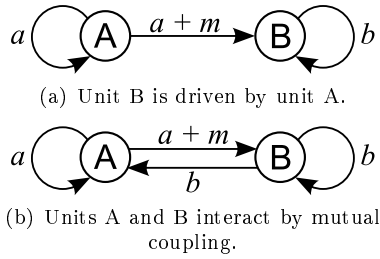


FIG. 1: Two different scenarios with two chaotic units. The states of units A and B are indicated by a and b , the exchanged small message by m .

with corresponding experiments on chaotic semiconductor lasers, we add a self-feedback to each of the two units, again with a delay time [4, 20, 21]. We compare two different scenarios, indicated in Fig. 1: (a) Unit B is driven by unit A, and (b) units A and B interact by a mutual coupling. For both cases, unit A is sending some message m to its partner B. This message is small and its content may be considered as small random noise. Thus we are interested in the linear response of unit B to noise.

In the following, we investigate the two scenarios with chaotic iterated maps [11, 22]. The dynamics is given by

- case (a) of Fig. 1

$$\begin{aligned} a_t &= (1 - \varepsilon)f(a_{t-1}) + \varepsilon f(a_{t-\tau}) \\ b_t &= (1 - \varepsilon)f(b_{t-1}) \\ &\quad + \varepsilon \kappa f(b_{t-\tau}) + \varepsilon(1 - \kappa)f(a_{t-\tau} + m_{t-\tau}), \end{aligned} \quad (1)$$

- case (b) of Fig. 1

$$\begin{aligned} a_t &= (1 - \varepsilon)f(a_{t-1}) \\ &\quad + \varepsilon \kappa f(a_{t-\tau}) + \varepsilon(1 - \kappa)f(b_{t-\tau}) \\ b_t &= (1 - \varepsilon)f(b_{t-1}) \\ &\quad + \varepsilon \kappa f(b_{t-\tau}) + \varepsilon(1 - \kappa)f(a_{t-\tau} + m_{t-\tau}). \end{aligned} \quad (2)$$

There are two parameters: ε measures the contribution of all delay terms while κ measures the relative strength of the self-feedback. For the function f we mainly use two variants:

- the Bernoulli shift

$$f(x) = \frac{3}{2}x \pmod{1} \quad (3)$$

and

- the logistic map

$$f(x) = 4x(1 - x) \quad (4)$$

Note that all variables a_t, b_t are iterated in the unit interval $[0, 1]$.

Without noise, $m_t = 0$, the spectra of Lyapunov exponents have been calculated for the Bernoulli system. In

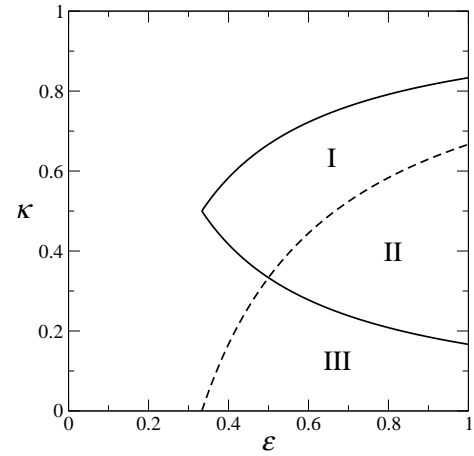


FIG. 2: Phase diagram for Bernoulli units. Regions II + III (- -): synchronization of A and B for case (a), see Eq. (5); regions I + II (—): synchronization for case (b), see Eq. (6).

the limit of large delay, $\tau \rightarrow \infty$, the phase diagram has been calculated analytically [22, 23]. In the stationary state, the two units A and B are completely synchronized for

$$\kappa < \frac{6\varepsilon - 2}{6\varepsilon} \quad \text{case (a),} \quad (5)$$

$$\frac{1}{6\varepsilon} < \kappa < \frac{6\varepsilon - 1}{6\varepsilon} \quad \text{case (b).} \quad (6)$$

These regions are shown in Fig. 2.

The uni-directional system synchronizes in regions II and III and the bi-directional in regions I and II. Synchronization is complete, $a_t = b_t$, although the exchanged signal has a very long delay.

The effect of small noise can be calculated by linearizing equations (1) and (2) in the vicinity of the synchronization manifold $a_t = b_t$. The noise leads to a small deviation $d_t = b_t - a_t$ which is given by the linear equations

- case (a)

$$\begin{aligned} d_t &= (1 - \varepsilon)f'_{t-1}d_{t-1} + \varepsilon \kappa f'_{t-\tau}d_{t-\tau} \\ &\quad + \varepsilon(1 - \kappa)f'_{t-\tau}m_{t-\tau}, \end{aligned} \quad (7)$$

- case (b)

$$\begin{aligned} d_t &= (1 - \varepsilon)f'_{t-1}d_{t-1} + \varepsilon \kappa f'_{t-\tau}d_{t-\tau} \\ &\quad + \varepsilon(1 - \kappa)f'_{t-\tau} \cdot (m_{t-\tau} - d_{t-\tau}) \\ &= (1 - \varepsilon)f'_{t-1}d_{t-1} + (2\kappa - 1)\varepsilon f'_{t-\tau}d_{t-\tau} \\ &\quad + \varepsilon(1 - \kappa)f'_{t-\tau}m_{t-\tau} \end{aligned} \quad (8)$$

where f'_t is the derivative of $f(x)$ at the synchronized trajectory $a_t = b_t$. Without noise, these equations determine the region of synchronization. For the Bernoulli system one has $f'_t = 3/2$ where we can ignore the jumps in the limit of infinitesimally small differences d_t . In this

case (and without noise), the equations have been solved analytically and determine the phase diagram of Fig. 2. In the synchronized regions, d_t decays to zero whereas outside d_t increases exponentially.

III. LINEAR RESPONSE

The transmitted message may be considered as noise with a low amplitude. Hence we want to understand how a synchronized chaotic system responds to small noise. In particular, we are interested in the linear response.

A. Moments

The distance from the synchronization manifold is described by the variable d_t of equations (7) and (8). We consider the regime of complete synchronization, i.e. parameters for which, without noise, d_t decays to zero. With noise, however, one obtains a distribution of distances d_t . We are interested in the stationary distribution which develops after a transient time given by the transverse Lyapunov exponents. This distribution may be characterized by its moments. Hence, we define a response function

$$\chi_n = \lim_{\langle |m| \rangle \rightarrow 0} \frac{\langle |d|^n \rangle}{\langle |m|^n \rangle}, \quad (9)$$

where $\langle \dots \rangle$ means an average over the distribution of m and d . In the following we will use a symmetric distribution of random numbers m_t , for example with a uniform distribution in the interval $[-M, M]$.

Let us consider the simplest case, Fig. 1(a) with $\tau = 1$ and $\kappa = 0$. The chaotic unit A is driving unit B. The linearized equation (7) takes the simple form

$$d_t = (1 - \varepsilon)f'_{t-1}d_{t-1} + \varepsilon f'_{t-1}m_{t-1}. \quad (10)$$

Let us assume that the variable f'_{t-1} is an uncorrelated random number. Then this equation describes a linear process with multiplicative and additive noise. For the Bernoulli shift, $f'_t = \frac{3}{2}$ is constant and only additive noise remains. But for the logistic map, the distribution of f' is given by

$$\rho(f') = \frac{1}{\pi\sqrt{16 - f'^2}}. \quad (11)$$

It is well known that linear systems with multiplicative and additive noise may lead to stationary distributions which have a power law [19, 24, 25]

$$p(d) \sim \frac{1}{d^\gamma}. \quad (12)$$

The exponent γ is determined by

$$(1 - \varepsilon)^{\gamma-1} \langle |f'_t|^{\gamma-1} \rangle = 1. \quad (13)$$

Hence, if the factor $(1 - \varepsilon)|f'_t|$ can take values larger than one, the equation (10) may drive the system to very large excursions, leading to a power law of the distribution. For the logistic map, the maximal slope is $f' = \pm 4$, thus we find large excursions of the variable d_t for $\varepsilon < \frac{3}{4}$. We did not succeed to calculate the distribution of d_t analytically, but the linear response can be derived.

Squaring equation (10), one finds the second moment of the deviation from synchronization as

$$\langle d^2 \rangle = \frac{\varepsilon^2 \langle f'^2 \rangle \langle m^2 \rangle}{1 - (1 - \varepsilon)^2 \langle f'^2 \rangle}. \quad (14)$$

For the Bernoulli shift, the second moment diverges for $\varepsilon < \varepsilon_c = \frac{1}{3}$ where synchronization does not occur. For the logistic map, however, the second moment diverges already inside of the synchronization region. Synchronization is given for

$$\ln(1 - \varepsilon) + \langle \ln |f'| \rangle < 0 \quad (15)$$

which gives $\varepsilon_c = \frac{1}{2}$. The second moment diverges when the denominator of equation (14) becomes negative. Since one has $\langle f'^2 \rangle = 8$, the second moment diverges for

$$\varepsilon < \varepsilon_2 = 1 - \frac{1}{\sqrt{8}} = 0.646 \dots \quad (16)$$

The second moment diverges already inside the region of synchronization. That means that the distribution $p(d)$ has developed a power law tail, and equation (10) describes rare large excursions of deviation d_t from the synchronization manifold. Figure 3 shows a trajectory of d_t for $\varepsilon = 0.7$ (b) where the second moment exists and for $\varepsilon = 0.6$ (a) where the susceptibility χ_2 diverges.

Power law tails of the distribution of a stochastic process with multiplicative and additive noise have been discussed in the context of chaos synchronization, before [2]. This phenomenon has been called ‘‘on-off intermittency’’ and was discussed in the vicinity of the synchronization transition ε_c . Here the phenomenon is triggered by the message transmitted via the chaotic signal, and it is observed deep inside the region of synchronization.

The linear equation (10) also determines higher moments of $p(d)$. Equation (13) shows that χ_n diverges at a coupling ε_n given by the equation

$$1 = (1 - \varepsilon_n)^n \langle |f'|^n \rangle \quad (17)$$

For the Bernoulli shift, all moments diverge at the synchronization threshold ε_c . For the logistic map, however, all moments diverge at a different coupling ε_n given by

$$\varepsilon_n = 1 - \frac{1}{4} \left(\frac{n\sqrt{\pi}\Gamma(\frac{n}{2})}{2\Gamma(\frac{n+1}{2})} \right)^{\frac{1}{n}} \quad (18)$$

Decreasing ε , the susceptibility χ_∞ diverges first. Then, at each value of ε , a susceptibility with a lower value of n diverges until for $n \rightarrow 0$ the synchronization threshold is obtained, where $(\ln |d|)$ diverges. Figure 4 shows ε_n as a

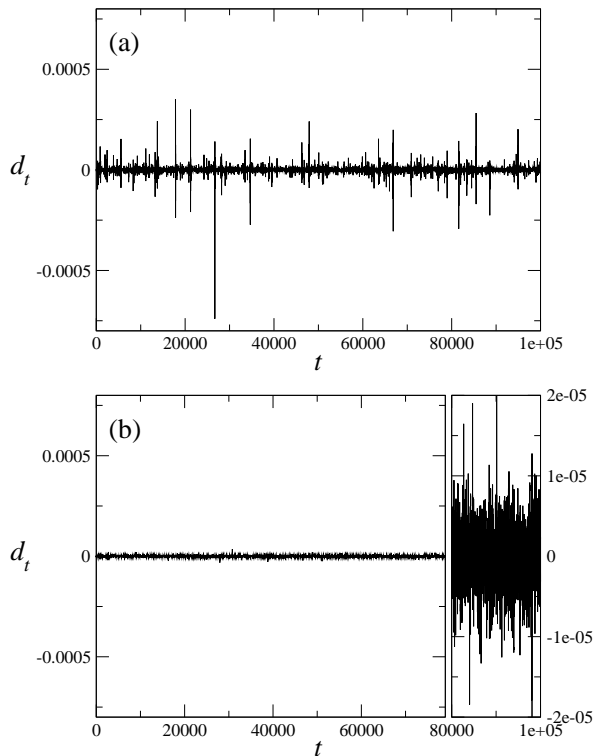


FIG. 3: Deviation d_t from the synchronization manifold for logistic map. (a) $\varepsilon = 0.6$: large excursions, χ_2 diverges; (b) $\varepsilon = 0.7$: χ_2 exists. Note the different scale in the second part of (b).

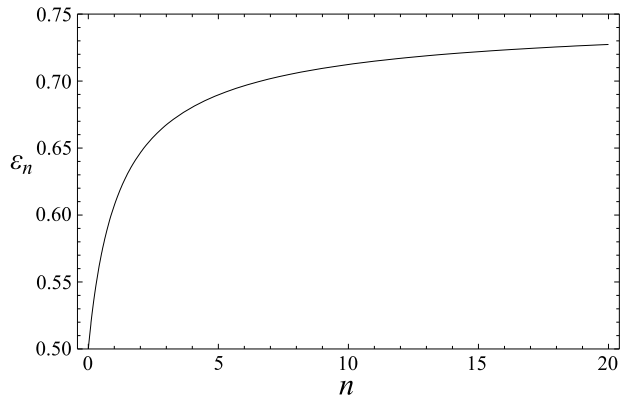


FIG. 4: The threshold ε_n below which χ_n diverges.

function of n . Note that Fig. 4 shows the exponent $\gamma(\varepsilon)$ as well since one has $\gamma = n + 1$.

Figure 5 shows the power-law of the probability distribution $p(d)$ of the distance d in a log-log plot for $\varepsilon = 0.65$. In addition, the straight line corresponding to the exponent γ is shown. It can be determined by Eq. (18) (Fig. 4) and $\gamma = n + 1$.

Up to now we have discussed the driven system, Fig. 1(a). But the linearized equations for the interacting system, Fig. 1(b), are very similar:

$$d_t = (1 - 2\varepsilon)f'_{t-1}d_{t-1} + \varepsilon f'_{t-1}m_{t-1} \quad (19)$$

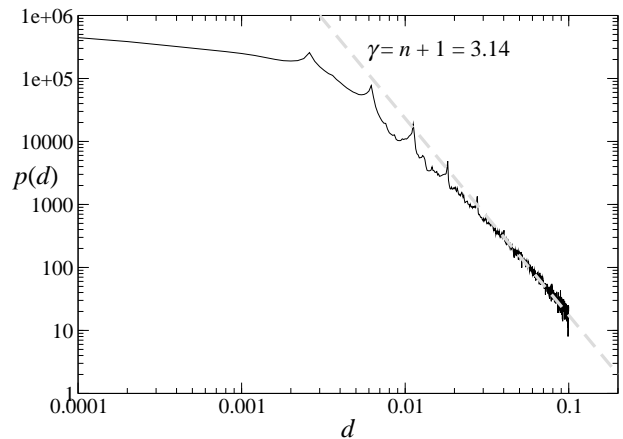


FIG. 5: Log-log plot of $p(d)$, the histogram of the distances, for the logistic map, uni-directional scenario, $\tau = 1$, $\varepsilon = 0.65$. Besides the small deviations from a perfect power-law for $d \approx 0.01$, there are two cut-offs: The first cut-off is for small d . It results from the additive noise which prevents that the distance very often becomes very small. The second cut-off is for large d . It results from the fact that $|d|$ is bounded between 0 and 1 (since a and b are bounded between 0 and 1) which means that d cannot really diverge.

Hence, in this case, one finds diverging susceptibilities, as well. For the logistic map, the region of synchronization is given by

$$\frac{1}{4} < \varepsilon < \frac{3}{4} \quad (20)$$

and χ_n diverges at

$$\varepsilon_n = \frac{1}{2} \pm \frac{1}{8} \left(\frac{n \sqrt{\pi} \Gamma(\frac{n}{2})}{2 \Gamma(\frac{n+1}{2})} \right)^{\frac{1}{n}} \quad (21)$$

Fig. 6 shows χ_2 as a function of ε . It diverges at the coupling strength $\varepsilon_2 = \{\frac{1}{2} \pm \frac{1}{4\sqrt{2}}\} = \{0.323 \dots, 0.676 \dots\}$. With increasing coupling, the effect of the noise becomes stronger, hence the susceptibility is not symmetric around $\varepsilon = 0.5$.

Up to now we have considered a system without delay. Now we are discussing the complete equations (7) and (8). If the delay time τ is very large, the variables d_{t-1} and $d_{t-\tau}$ may be considered as uncorrelated random variables. Hence the second moment diverges when the following inequalities hold:

- Uni-directional

$$1 - [(1 - \varepsilon)^2 + \varepsilon^2 \kappa^2] \langle f'^2 \rangle < 0 \quad (22)$$

- Bi-directional

$$1 - [(1 - \varepsilon)^2 + \varepsilon^2 (2\kappa - 1)^2] \langle f'^2 \rangle < 0 \quad (23)$$

For the Bernoulli shift one has $f' = \text{const.} = \frac{3}{2}$ and all moments diverge at the synchronization threshold.

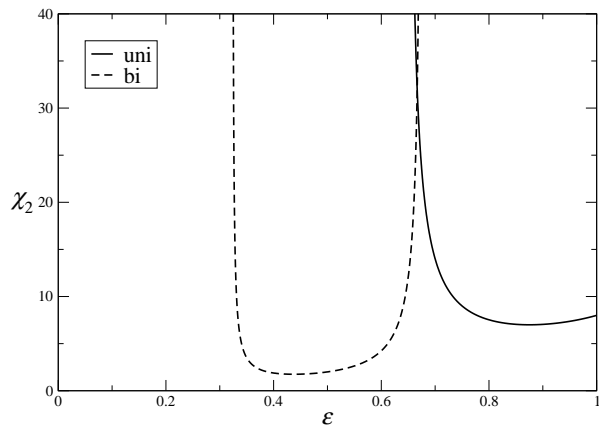


FIG. 6: The susceptibility χ_2 as a function of ε in the case of uni- and bi-directional coupling and $\tau = 1$ for the logistic map.

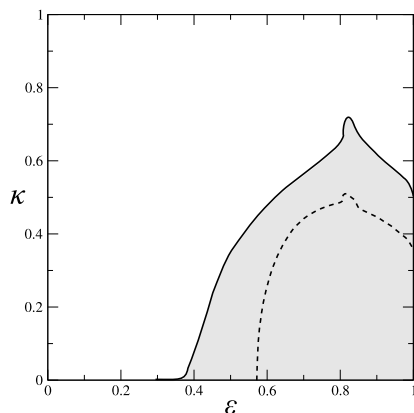


FIG. 7: Phase diagram for the unidirectional setup, the logistic map and $\tau \rightarrow \infty$, obtained from numerical simulations. The gray regime with black border (—) shows the synchronization region. The dashed line (- -) confines the region outside which χ_2 diverges. That is, the divergence already occurs inside the synchronization region.

For the logistic map, however, these equations cannot be solved analytically since the distribution of f' is not known. Figure 7 shows a numerical simulation which demonstrates that the susceptibility χ_2 already diverges inside of the synchronization region.

B. Bit Error Rate

In the following, we assume that A sends binary messages (bits), i.e. $m_t = \pm M$ with $M \ll 1$ and $\langle m \rangle = 0$. To reconstruct the small message m which A sends to B, unit B first has to subtract its own state from the received signal [11]:

$$\tilde{m}_t = (a_t + m_t) - b_t = m_t - d_t. \quad (24)$$

If units A and B were perfectly synchronized ($d_t = 0$), the original message would be perfectly recovered by the

above equation ($\tilde{m}_t = m_t$). But since the original message is binary ($\pm M$), it is sufficient for a successful reconstruction if m_t and \tilde{m}_t have the same sign, $m_t \tilde{m}_t > 0$. To measure the quality of reconstruction, the bit error rate (BER) r is introduced, which is the ratio of the number of incorrectly recovered bits to the total number of received bits:

$$r = \frac{\# \text{ incorrectly recovered bits}}{\# \text{ received bits}}. \quad (25)$$

If the absolute value of the distance d is less than the absolute value of the messages, $|d_t| < M$, the message is recovered correctly with probability 1 because the sign of the message is not changed. In the other cases, $|d_t| > M$, the sign of the message is changed with probability $\frac{1}{2}$, i.e.

$$\begin{aligned} r &= \frac{1}{2} \left(\int_{-\infty}^{-M} p(d) dd + \int_M^{\infty} p(d) dd \right) \\ &= \frac{1}{2} \left(1 - \int_{-M}^M p(d) dd \right). \end{aligned} \quad (26)$$

Note that this definition of the bit error rate assumes that the system has relaxed to a stationary distribution $p(d)$. In fact, this definition may be only an upper bound since lower bit error rates may be achievable if one uses additional information about the transmitted signals [26].

The distribution of the distances, $p(d)$, is known analytically only in some special cases, see Appendix. In general, the bit error rate has to be determined by means of computer simulations. Figures 8, 9, 10 and 11 show the results of simulations for the uni-directional/bi-directional setup, for the Bernoulli map/logistic map and for no delay/large delay.

For the Bernoulli map without delay, Fig. 8, we find a broad distribution of deviations d for small ε in the case of uni-directional coupling, see Fig. 12(a). With increasing ε , Fig. 12(b), the values of the distribution get a fractal structure while the support stays connected. For $\varepsilon > \frac{2}{3}$, Fig. 12(c), the distribution changes to a peaked structure with a fractal support. As derived in the Appendix, this fractal structure leads to a devil's staircase for the bit error rate as a function of ε . The bit error rate locks into rational values $r = \frac{k}{2^q}$ with k and q being natural numbers and $\frac{1}{4} \leq r \leq \frac{1}{2}$. In the bi-directional case, the bit error rate is zero for $\frac{1}{3} \leq \varepsilon \leq \frac{5}{9}$ since for this interval the absolute values of the deviations are less than the message amplitude, $|d| < M$, see Fig. 12(d). Similarly to the uni-directional case, one can find a staircase structure for the bit error rate for $\frac{1}{3} \leq \varepsilon \leq \frac{2}{3}$. The fractal properties of the distribution $p(d)$ are related to the theory of iterated function systems [27]. For the Bernoulli shift, Eqs. (10) and (19) give iterations of two linear functions with $m_{t-1} = \pm 1$. Iterating a few randomly chosen functions can lead to fractal distribution. For details see Appendix.

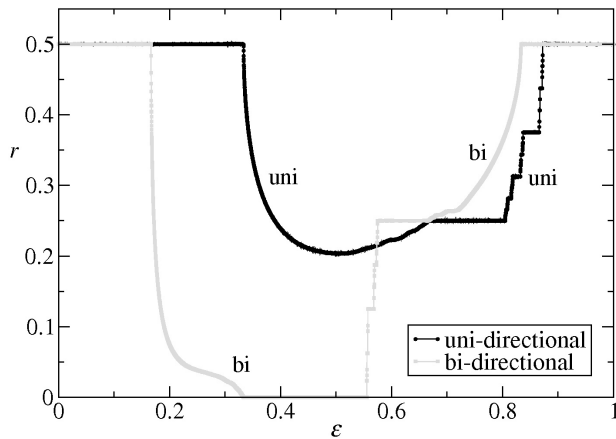


FIG. 8: Bit error rate r for Bernoulli map, $\tau = 1$, $\kappa = 0$, for uni- and bi-directional coupling.

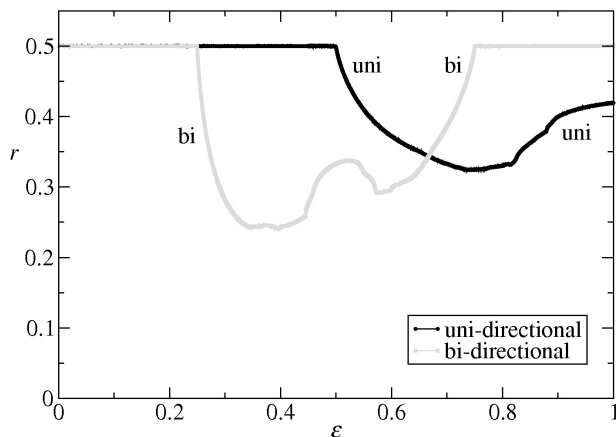


FIG. 9: Bit error rate r for logistic map, $\tau = 1$, $\kappa = 0$, for uni- and bi-directional coupling.

For the logistic map without delay, Fig. 9, the distribution $p(d)$ of deviations d has always a connected support due to the multiplicative noise f' , see Figures 12(e) and (f). The numerical simulations show a minimum of the bit error rate at $\varepsilon \simeq 0.75$ (uni-directional case) and $\varepsilon \simeq 0.4$ (bi-directional case).

Note that the bit error rate is determined by the integral (26) of the distribution of distances d from the synchronization manifold. We find that this integral is insensitive to long tails of this distribution, discussed in the previous subsection. Although the responses χ_n diverge at different coupling strengths ε_n , the bit error rate is smooth as a function of ε .

In the sequence of correctly and incorrectly recovered bits, there are correlations between time steps with a distance Δ of integer multiples of τ and close to integer multiples, i.e. $\Delta \approx k\tau$ with $k = \dots, -2, -1, 0, 1, 2, \dots$, e.g. $\Delta = 1$, $\Delta = 2\tau - 2$, \dots . An example can be seen in Fig. 13. For short time shifts Δ , the bit errors are not correlated. But this does not necessarily mean that the bit error rate can always be reduced by using larger bits

(bits longer than one time step), since the system immediately responds to a long constant perturbation, i.e. the errors each time step are not independent anymore if the bits are longer than one time step. However, in most of the cases the bit error rate *is* reduced by using longer bits, as seen in Fig. 14.

C. Noise-reduced bit error rate

In the previous subsections we have investigated the case where a message $m_t = \pm M$ is added to the signal which unit A sends to B, and we have calculated the response of unit B. This response was quantified with the bit error rate r^B .

Now we extend this scenario to the case where unit B adds noise w (or a message) to its transmitted signal as well,

$$\begin{aligned} a_t &= (1 - \varepsilon)f(a_{t-1}) \\ &\quad + \varepsilon\kappa f(a_{t-\tau}) + \varepsilon(1 - \kappa)f(b_{t-\tau} + w_{t-\tau}) \\ b_t &= (1 - \varepsilon)f(b_{t-1}) \\ &\quad + \varepsilon\kappa f(b_{t-\tau}) + \varepsilon(1 - \kappa)f(a_{t-\tau} + m_{t-\tau}), \end{aligned} \quad (27)$$

see also Fig. 15. Surprisingly, we find that this additional noise can reduce the bit error rate r^B .

This effect can be seen with the Bernoulli map as well as with the logistic map for many of the possible choices of the parameters in Eq. (27). However, to treat the effect analytically, we set $\tau = 1$, $\kappa = 0$, $\varepsilon = \frac{1}{2}$. The corresponding equations are

$$\begin{aligned} a_t &= \frac{1}{2}f(a_{t-1}) + \frac{1}{2}f(b_{t-1} + w_{t-1}) \\ b_t &= \frac{1}{2}f(b_{t-1}) + \frac{1}{2}f(a_{t-1} + m_{t-1}) \end{aligned} \quad (28)$$

Let us consider the case of the logistic map. Obviously, for the above choice of parameters A and B synchronize immediately when the message m_t and the noise w_t are switched off. When message and noise are small, the deviation from the synchronous trajectory is obtained from the linearized equations. With $b_t = a_t + d_t$ one finds

$$d_t = \frac{f'_{t-1}}{2}(m_{t-1} - w_{t-1}) \quad (29)$$

where f'_{t-1} is the derivative of the nonlinear function f at the perturbed trajectory a_t ; it may be considered as a random number. In the case of the logistic map, Eq. (4), the distribution of $s = f'/2$ is given by

$$\tilde{\rho}(s) = \frac{1}{\pi\sqrt{4-s^2}} \quad (30)$$

The unit B recovers the message from the sign of

$$m_t^B = a_t + m_t - b_t = m_t - d_t. \quad (31)$$

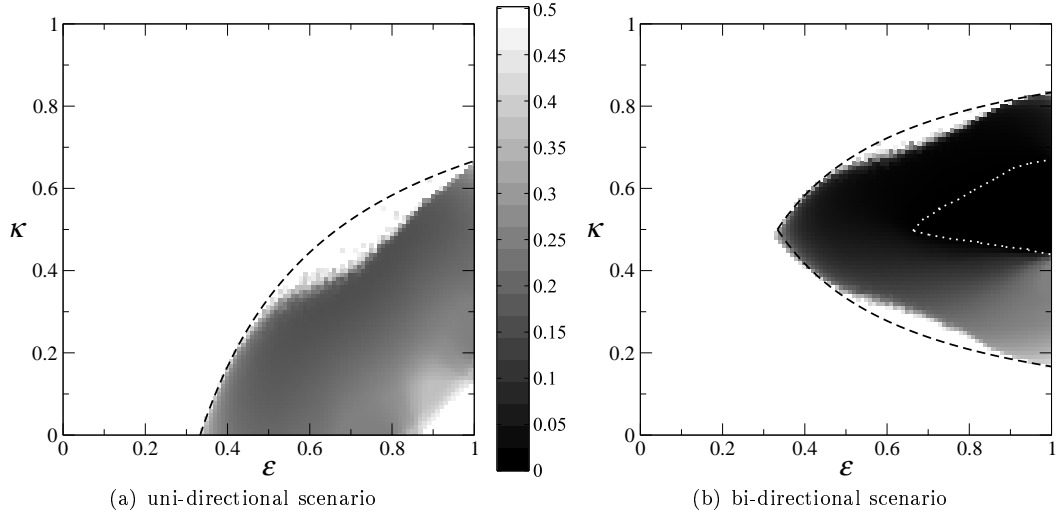


FIG. 10: Bit error rate r (gray-scale) for Bernoulli map, $\tau = 50$. The dashed lines (--) represent the borders of the synchronization regions, see Fig. 2. The white dotted line (··) in (b) confines the region where $r < 10^{-4}$.

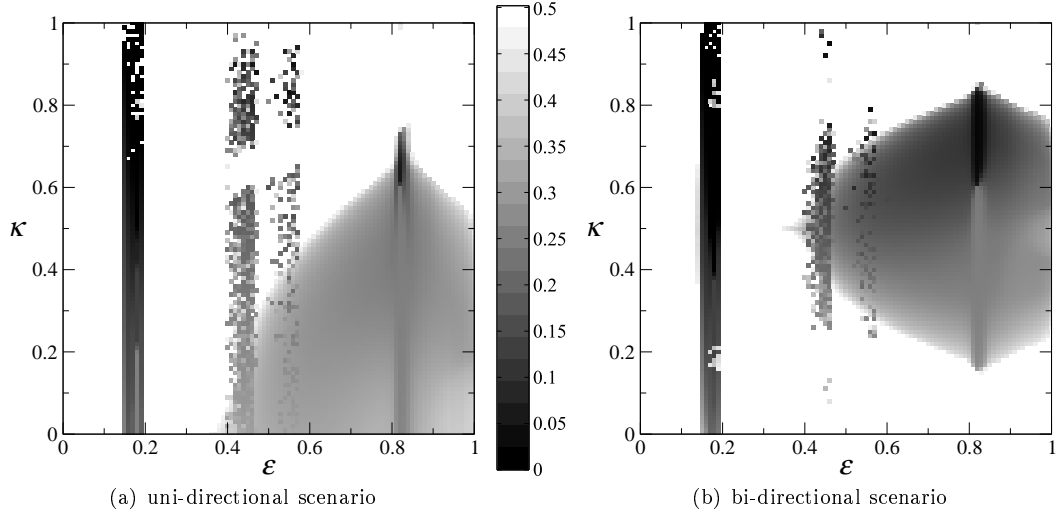


FIG. 11: Bit error rate r (gray-scale) for logistic map, $\tau = 50$. The bands around $\varepsilon \simeq 0.15$, 0.45 and 0.55 represent periodic windows.

The bit error rate of B is given by

$$\begin{aligned}
r^B &= \text{prob}(m_t m_t^B < 0) \\
&= \text{prob}(M^2 - s_{t-1}M^2 + s_{t-1}w_{t-1}m_t < 0) \\
&= \text{prob}(M - s_{t-1}M \pm s_{t-1}w_{t-1} < 0) \\
&= \text{prob}(M - s(M+w) < 0) \\
&= \int_{-\frac{M}{2}}^{\infty} p_w(w) \int_{\frac{M}{M+w}}^2 \tilde{\rho}(s) ds dw \\
&\quad + \int_{-\infty}^{-\frac{3}{2}M} p_w(w) \int_{-\frac{M}{M+w}}^2 \tilde{\rho}(s) ds dw \\
&= \left(\int_{-\infty}^{-\frac{3}{2}M} + \int_{-\frac{M}{2}}^{\infty} \right) \frac{1}{\pi} \sec^{-1} \left(2 \left| 1 + \frac{w}{M} \right| \right) p_w(w) dw
\end{aligned} \tag{32}$$

For small values of the noise, $\frac{w}{M} \ll 1$, one can expand the inverse sec; for a symmetric distribution of noise one finds

$$r^B = \frac{1}{3} - \frac{7\langle w^2 \rangle}{6\sqrt{3}M^2\pi} - \frac{205\langle w^4 \rangle}{108\sqrt{3}M^4\pi} + O(\langle w^6 \rangle) \tag{33}$$

For large noise we have calculated the integral (32) for a flat distribution, $w \in [-W, W]$ with $p_w(w) = \frac{1}{2W}$. The result is given in Appendix B, and Fig. 16 shows the bit error rate $r^B(W)$ as a function of noise W . If unit B adds noise to its transmitted signal, it reduces its bit error rate. Only when the ratio between maximal noise W to the strength of the bit message M is larger than the value ≈ 3.4 , B has a larger error rate than without noise.

As mentioned before, the effect of decreasing the bit

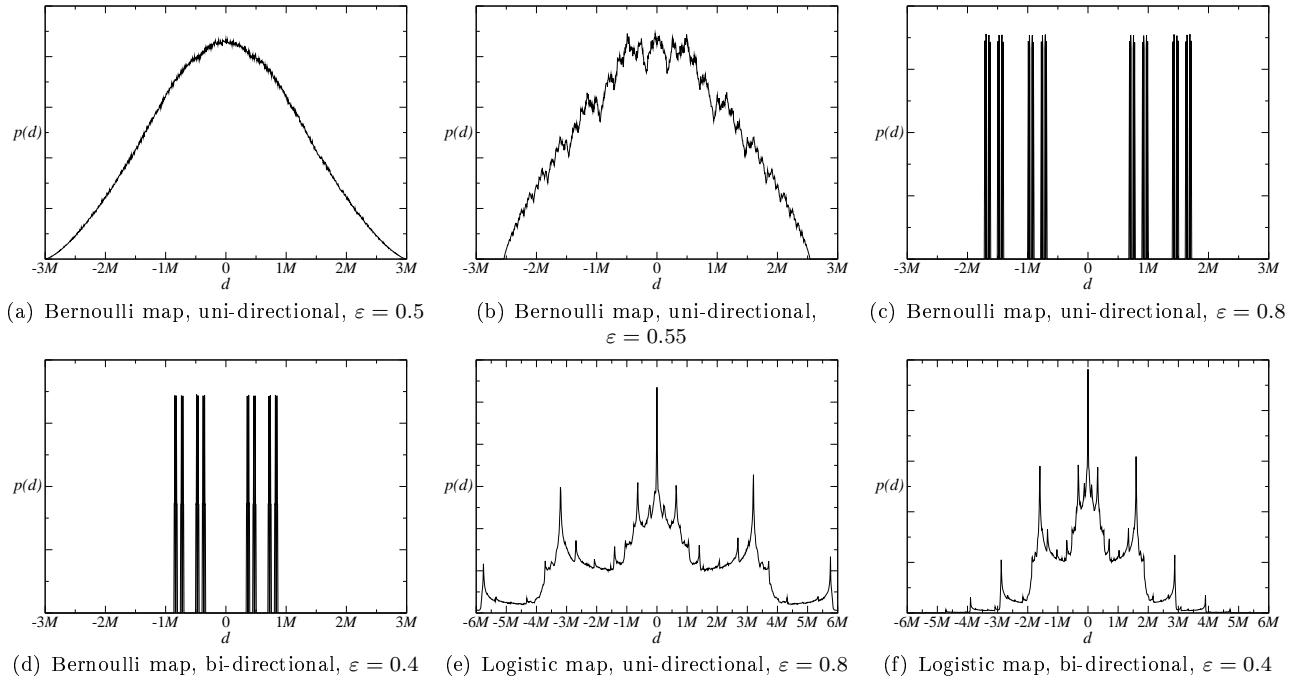


FIG. 12: Probability distribution $p(d)$ (in arb. units) for the deviations d with $\tau = 1$, $\kappa = 0$.

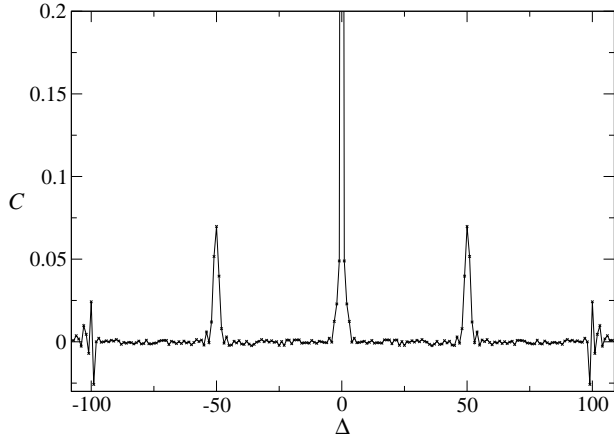


FIG. 13: Auto-correlation C with time shift Δ of the sequence of correctly and incorrectly recovered bits, $C = \frac{(c_t c_{t-\Delta}) - \langle c \rangle^2}{(\langle c^2 \rangle - \langle c \rangle^2)}$, $c_t = +1$: correctly recovered bit, $c_t = -1$: incorrectly recovered bit. Logistic map, bi-directional scenario, $\tau = 50$, $\varepsilon = 0.7$, $\kappa = 0.6$.

error rate by noise exists not only for the special case of Eq. (28) but also for the more general case of Eq. (27) with delay and feedback (in certain regions of the parameter space), both for the Bernoulli map and for the logistic map. This is shown in Figures 17 and 18.

In order to explain the positive effect of noise, let us go back to the special case of Eq. (28) and the logistic map. Consider the case where there is a bit error without noise. According to Eq. (29), with $w_t = 0$, one has $|f'| > 2$. In this case noise can reduce the value of d_t and remove

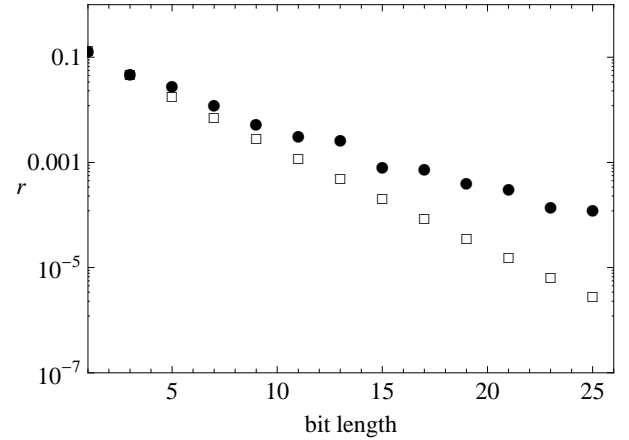


FIG. 14: Bit error rate (●) as a function of the bit length for logistic map, bi-directional scenario, $\tau = 50$, $\varepsilon = 0.7$, $\kappa = 0.6$. For bit lengths > 1 , the bit error rate deviates from a behavior (□) of independent bit errors (binomial sum).

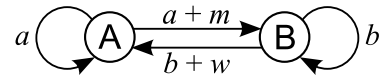


FIG. 15: B sends noise w in addition to the signal b .

the bit error. Noise can also generate a bit error when $|f'| < 2$. But since the distribution of $|f'|$ is increasing, the probability of the first case is larger, resulting in a reduction of the total bit error rate.

The main idea of this explanation for the special case

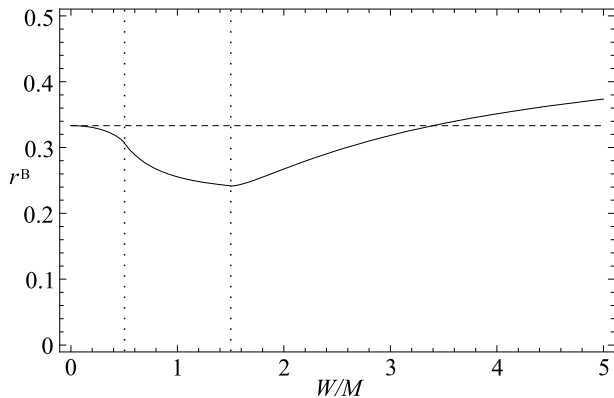


FIG. 16: Bit error rate r^B for different strengths W of the noise $w \in [-W, W]$ with flat distribution $p_w(w) = \frac{1}{2W}$ which B sends in addition to the signal b . Surprisingly, the bit error rate decreases due to the noise. The analytical result for the logistic map with $\tau = 1$, $\kappa = 0$ and $\varepsilon = \frac{1}{2}$ is shown. The horizontal dashed line represents the bit error rate without noise, $W = 0$.

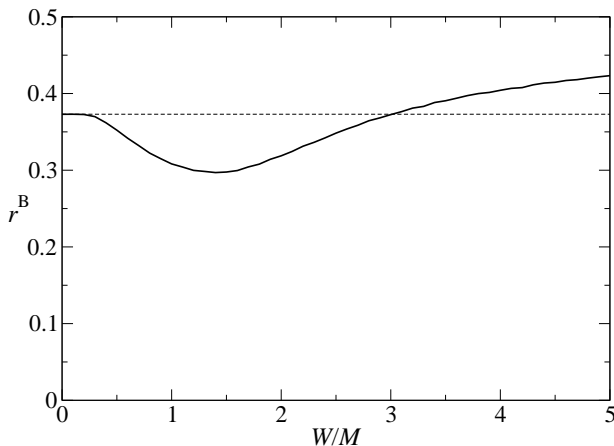


FIG. 17: Bit error rate r^B for different strengths W of the noise $w \in [-W, W]$ with flat distribution $p_w(w) = \frac{1}{2W}$. Result from simulation for Bernoulli map $f(x) = \alpha x \bmod 1$ with $\alpha = \frac{5}{2}$, $\varepsilon = 0.95$, $\kappa = 0.45$, $\tau = 50$. The dashed line represents the bit error rate without noise, $W = 0$.

also holds for the general case of Eq. (27): If the probability density $p(d)$ without noise prevails in the region $|d| > M$, changing d by noise leads to an increasing of the probability density within the interval $|d| < M$ which decreases the bit error rate.

D. Resonances

In the previous subsection we have investigated the linear response of synchronized chaotic units to a random perturbation m_t . The response was described by the functions χ_n , Eq. (9). For the Bernoulli map, the corresponding equations (7) and (8) are linear equations with constant coefficients. Hence, in this special case, the re-

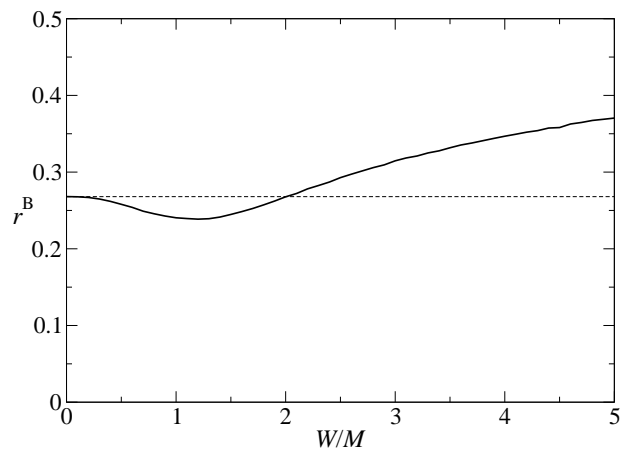


FIG. 18: Bit error rate r^B for different strengths W of the noise $w \in [-W, W]$ with flat distribution $p_w(w) = \frac{1}{2W}$. Result from simulation for logistic map, $\varepsilon = 0.9$, $\kappa = 0.4$, $\tau = 50$. The dashed line represents the bit error rate without noise, $W = 0$.

sponse of the chaotic system can be described in terms of harmonic perturbations $m_t = M \exp(-i\omega t)$. The system responds with the identical frequency $d_t = D \exp(-i\omega t)$, and the complex amplitude D is given by

- uni-directional case

$$D = M \frac{\varepsilon(1 - \kappa)\alpha}{\exp(i\omega\tau) - (1 - \varepsilon)\alpha \exp(i\omega(\tau - 1)) - \varepsilon\kappa\alpha} \quad (34)$$

- bi-directional case

$$D = M \frac{\varepsilon(1 - \kappa)\alpha}{\exp(i\omega\tau) - (1 - \varepsilon)\alpha \exp(i\omega(\tau - 1)) - \varepsilon(2\kappa - 1)\alpha} \quad (35)$$

with $\alpha = f' = \frac{3}{2}$. The unit A sends the harmonic signal m_t and the unit B tries to recover it by subtracting its own variable b_t from the received signal $a_t + m_t$. The recovered signal is $\tilde{m} = a_t + m_t - b_t = m_t - d_t$. Hence the amplitude of the recovered signal is given by

$$|\tilde{m}| = |M - D| \quad (36)$$

Figure 19 shows $|\tilde{m}|$ as a function of ω close to the phase boundary of synchronization. The amplitude of the restructured signal shows peaks (resonances) and/or cuts with distance $\frac{2\pi}{\tau}$. The resonances diverge at the synchronization boundary.

For the logistic map the coefficients of the linear equations (7) and (8) depend on time. Thus an exact Fourier decomposition of the transmitted signal is not possible. However, our numerical results of Fig. 20 show that the corresponding Fourier component of the response \tilde{m}_t shows resonances as well [28].

These results show that a chaotic system can function as a sharp harmonic filter. The transmitted signal is irregular, and the harmonic perturbation is arbitrarily small. Nevertheless, the receiver can filter out this

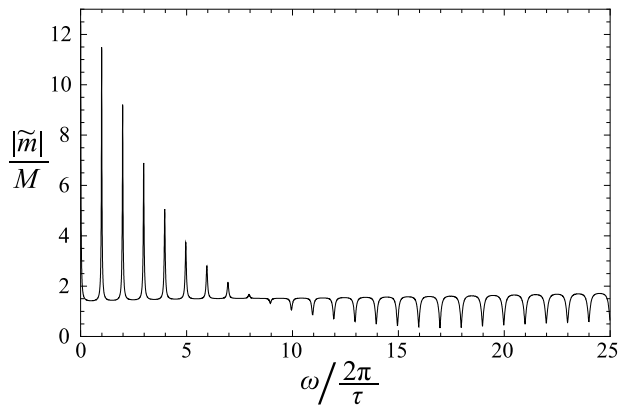


FIG. 19: Amplitude of the reconstructed signal for different signal frequencies. Bernoulli map, uni-directional coupling, $\varepsilon = 0.8$, $\kappa = 0.55$, $\tau = 50$.

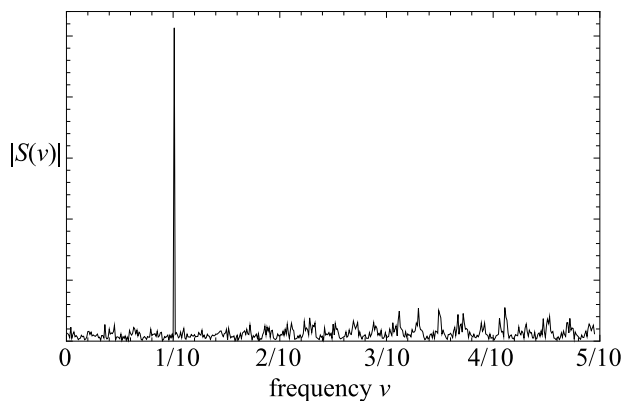


FIG. 20: Fourier transformation of the reconstructed signal, $S(\nu) = \sum_{t=1}^N \tilde{m}_t \exp[\frac{2\pi i}{N}(t-1)(N\nu-1)]$. Logistic map, uni-directional coupling, $\varepsilon = 0.7$, $\kappa = 0.4$, $\tau = 50$, $\omega = 2\pi \cdot \frac{5}{10}$. In the Fourier spectrum there is a strong peak at $\nu = \frac{5}{10} = \frac{1}{2}$ which corresponds to the frequency of the harmonic perturbation.

perturbation with high precision. It would be interesting to investigate this harmonic filter with respect to secret communication. In fact, the response of synchronized chaotic semiconductor lasers to a harmonic perturbation has been investigated in Ref. [29].

E. Transverse Lyapunov Spectra

In the previous subsections we have investigated the response of a synchronized chaotic system to persistent random or harmonic perturbations. The chaotic dynamic tries to bring the system to the synchronization manifold, whereas the perturbation drives the system away from this manifold. The competition between these two mechanisms results in the linear response described above.

The first mechanism – relaxation to the synchronization manifold – is usually described in terms of transverse or conditional Lyapunov exponents. In the synchronized

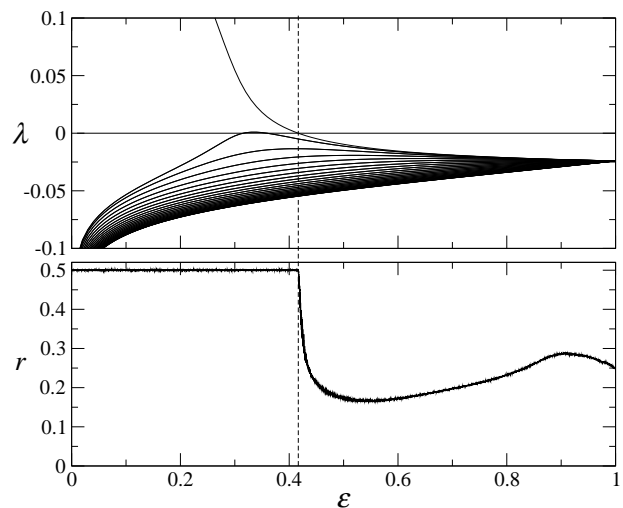


FIG. 21: Spectrum of transverse Lyapunov exponents λ and bit error rate r for Bernoulli map, uni-directional coupling, $\kappa = 0.2$, $\tau = 50$. Except for the synchronization boundary where the largest transverse Lyapunov exponent becomes negative and the bit error rate becomes less than $\frac{1}{2}$, the qualitative behavior of the Lyapunov exponents and the bit error rate are not related.

region those exponents are negative and the largest one becomes positive just at the phase boundary, resulting in a slowing down of the relaxation to synchronization. As we have seen above, at the phase boundary the response to perturbation diverges, as well.

Following these arguments, one might expect that the qualitative behavior of the response functions χ_n or the bit error rate r is related to the behavior of the largest transverse Lyapunov exponent λ_{trans} . However, this is not true. For example, consider the simple driven system without delay, Eq. (10). The transverse Lyapunov exponent is given by (15),

$$\lambda_{\text{trans}} = \ln(1 - \varepsilon) + \langle \ln |f'| \rangle. \quad (37)$$

Thus, it decreases monotonically with increasing coupling strength ε . However, the bit error rate r first decreases with ε to a minimum value but then it increases again. This holds for the Bernoulli as well as for the logistic map, see Figs. 8 and 9.

With delay τ , the spectra of Lyapunov exponents can be calculated by solving polynomial equations of order τ [22]. In Fig. 21 the spectrum of τ transverse exponents is shown as a function of ε for the self-feedback strength $\kappa = 0.2$. Again, the qualitative behavior of the largest exponent is not related to the one of the bit error rate r .

IV. ATTACKING WITH DRIVEN UNITS

The main motivation of this investigation is the application of chaos synchronization to secure communication. Let us assume that two partners A and B have realized

a synchronized chaotic system and transmit messages, as described above. But now an attacker E has access to the transmitted signal. We assume that the attacker can only record the transmitted signal, but he cannot send his own signal to the partners A and B. Thus E is driven by the transmitted signals but he cannot interact. This important difference between partners and attacking units has been suggested for a novel public key encryption protocol [4, 15].

To extract the message from the transmitted signals, the attacker has to synchronize with the two partners. Thus it is obvious that he will use the same chaotic units with identical parameters. If he does not know those parameters and if he is not able to estimate them from the data, he will not be able to synchronize. But secure cryptography does not use any secret parameters, hence we assume that the attacker E knows everything what B knows about A. In this case, the configuration of Fig. 1(a), A is driving B, is obviously useless, since E is in the same situation as B and can restore the message of A with identical precision as B.

Thus we consider only Fig. 1(b) where A and B are mutually interacting. The attacking unit E may have access to both transmission lines, as indicated in Fig. 22. The corresponding equation for the units A and B are given by Eq. (2), and E uses the equations:

$$e_t = (1 - \varepsilon)f(e_{t-1}) + \varepsilon\sigma f(b_{t-\tau}) + \varepsilon(1 - \sigma)f(a_{t-\tau} + m_{t-\tau}) \quad (38)$$

If unit E adjusts its parameter to $\sigma = \kappa$, it is obvious that unit E receives the identical drive including the same self-feedback as unit B. Consequently, E achieves an identical bit error rate.

The situation is different if B sends a message or noise as well. This scenario was investigated in Section III C. In this case and for $\tau = 1$, the equations for A, B and a simple attacker E are the following:

$$\begin{aligned} a_t &= (1 - \varepsilon)f(a_{t-1}) + \varepsilon f(b_{t-1} + w_{t-1}) \\ b_t &= (1 - \varepsilon)f(b_{t-1}) + \varepsilon f(a_{t-1} + m_{t-1}) \\ e_t &= (1 - \varepsilon)f(b_{t-1} + w_{t-1}) + \varepsilon f(a_{t-1} + m_{t-1}) \end{aligned} \quad (39)$$

From the above equations, the distance between A and B, d_t , and the distance between A and E, g_t , can be calculated:

$$\begin{aligned} d_t &= b_t - a_t \\ &= (1 - 2\varepsilon)f'_{t-1}d_{t-1} + \varepsilon f'_{t-1}m_{t-1} - \varepsilon f'_{t-1}w_{t-1} \\ g_t &= e_t - a_t \\ &= (1 - 2\varepsilon)f'_{t-1}d_{t-1} + \varepsilon f'_{t-1}m_{t-1} + (1 - 2\varepsilon)f'_{t-1}w_{t-1} \end{aligned} \quad (40)$$

If one sets $\varepsilon = \frac{1}{2}$, the bit error rate of B is reduced by the noise w , see Sec. III C, whereas the bit error rate of E is then independent of w and is not reduced (indicated by the dashed line in Fig. 16). This phenomenon has been reported for chaotic semiconductor lasers. A large difference in bit error rates for the partners and for the

attacker was observed for the Lang-Kobayashi equations describing chaotic semiconductor lasers. The effect was named “mutual chaos pass filter” [16].

However, for our simple model, an advanced attacker can achieve the same bit error rate as B. This should be shown for arbitrary ε . The equation of the advanced attacker is:

$$\begin{aligned} e_t &= (1 - 2\varepsilon)f(e_{t-1}) + \varepsilon f(a_{t-1} + m_{t-1}) \\ &\quad + \varepsilon f(b_{t-1} + w_{t-1}) - \varepsilon f'_{t-1}y_{t-1} \end{aligned} \quad (41)$$

Here, y is an additional noise with the same distribution as w , and f'_{t-1} can be calculated from a_{t-1} and b_{t-1} . For other maps than Bernoulli map and logistic map this might not be possible. Then it is sufficient to use values with the same distribution as f' . For the advanced attacker the distance between A and E is:

$$g_t = (1 - 2\varepsilon)f'_{t-1}g_{t-1} + \varepsilon f'_{t-1}m_{t-1} - \varepsilon f'_{t-1}y_{t-1} \quad (42)$$

which is identical to the equation for d_t and thus results in the same bit error rate.

An attacker is also successful if $\tau > 1$. The dynamics of units A and B and of an advanced attacker E are:

$$\begin{aligned} a_t &= (1 - \varepsilon)f(a_{t-1}) + \varepsilon\kappa f(a_{t-\tau}) \\ &\quad + \varepsilon(1 - \kappa)f(b_{t-\tau} + w_{t-\tau}) \\ b_t &= (1 - \varepsilon)f(b_{t-1}) + \varepsilon\kappa f(b_{t-\tau}) \\ &\quad + \varepsilon(1 - \kappa)f(a_{t-\tau} + m_{t-\tau}) \\ e_t &= (1 - \varepsilon)f(e_{t-1}) + \varepsilon(2\kappa - 1)f(e_{t-\tau}) \\ &\quad + \varepsilon(1 - \kappa)f(a_{t-\tau} + m_{t-\tau}) + \varepsilon(1 - \kappa)f(b_{t-\tau} + w_{t-\tau}) \\ &\quad - \varepsilon(1 - \kappa)f'_{t-\tau}y_{t-\tau} \end{aligned} \quad (43)$$

So the distance of the attacker to unit A, $g_t = e_t - a_t$, corresponds to the difference between A and B, $d_t = b_t - a_t$:

$$\begin{aligned} d_t &= (1 - \varepsilon)f'_{t-1}d_{t-1} + \varepsilon(2\kappa - 1)f'_{t-\tau}d_{t-\tau} \\ &\quad + \varepsilon(1 - \kappa)f'_{t-\tau}(m_{t-\tau} - w_{t-\tau}) \\ g_t &= (1 - \varepsilon)f'_{t-1}g_{t-1} + \varepsilon(2\kappa - 1)f'_{t-\tau}g_{t-\tau} \\ &\quad + \varepsilon(1 - \kappa)f'_{t-\tau}m_{t-\tau} - \varepsilon(1 - \kappa)f'_{t-\tau}y_{t-\tau} \end{aligned} \quad (44)$$

Again, if the attacker E is able to add additional noise y_t where $f'_t y_t$ has the same or similar distribution as $f'_t w_t$, he can reduce his bit error rate in a similar way as partner B.

Note that our results are based on iterated maps. For more complex systems, like the Lang-Kobayashi equations and other higher-dimensional chaotic systems, it is not obvious that the same conclusions about the mutual chaos pass filter hold.

Now let us come back to the general case $\tau > 1$ and let us assume that the attacker E is only able to record the transmission from A to B, see Fig. 23. For this case, the equation for E is

$$e_t = (1 - \varepsilon)f(e_{t-1}) + \varepsilon\sigma f(e_{t-\tau}) + \varepsilon(1 - \sigma)f(a_{t-\tau} + m_{t-\tau}) \quad (45)$$

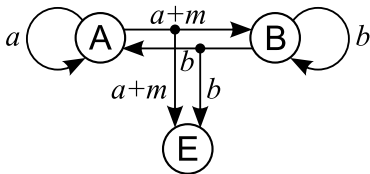


FIG. 22: The two units A and B are coupled as in Fig. 1(b). Here, an attacker E has access to both signals.

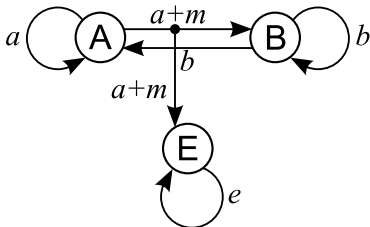


FIG. 23: The two units A and B are coupled as in Fig. 1(b). Here, an attacker E has access to the signal which goes from A to B.

We want to compare the linear response of unit E to the one of B. According to the phase diagram Fig. 2, without message, unit E can always synchronize to A and B if it uses an identical parameter ε and keeps its feedback parameter σ in region II or III.

Let us assume that A and B take their parameters (ε, κ) in region II. If the attacker E chooses $\kappa = \sigma$, he obtains the same response and bit error rate as B.

Figure 24(a) shows the second moment and bit error rate of E as a function of σ . Both quantities decrease monotonically with the feedback parameter σ . This result may be unexpected. One might expect that the attacker E obtains the lowest bit error rate if he uses a strong signal containing the message. The opposite is true, E can even achieve a lower bit error rate than B if he takes the almost weakest possible contribution of the signal without losing synchronization, here $\sigma \approx \frac{7}{12} = 0.58\bar{3}$ for $\varepsilon = \frac{8}{10} = 0.8$ according to Eq. (5). Only very close to the synchronization boundary the response χ_2^E diverges and the bit error rate increases to its maximal value $r^E = 0.5$.

If the two partners use parameters of region I, the attacker E can never achieve the same response as partner B. Figure 24(b) shows that the bit error rate as well as χ_2 of E is much larger than the ones of partner B. The bit error rate of E is always at least about 10 times larger than the one of B.

V. SUMMARY

Chaos synchronization has been investigated in the context of secure communication via chaotic signals. In particular, when a small secret message is a perturbation of the sending chaotic unit, the receiver can recover this

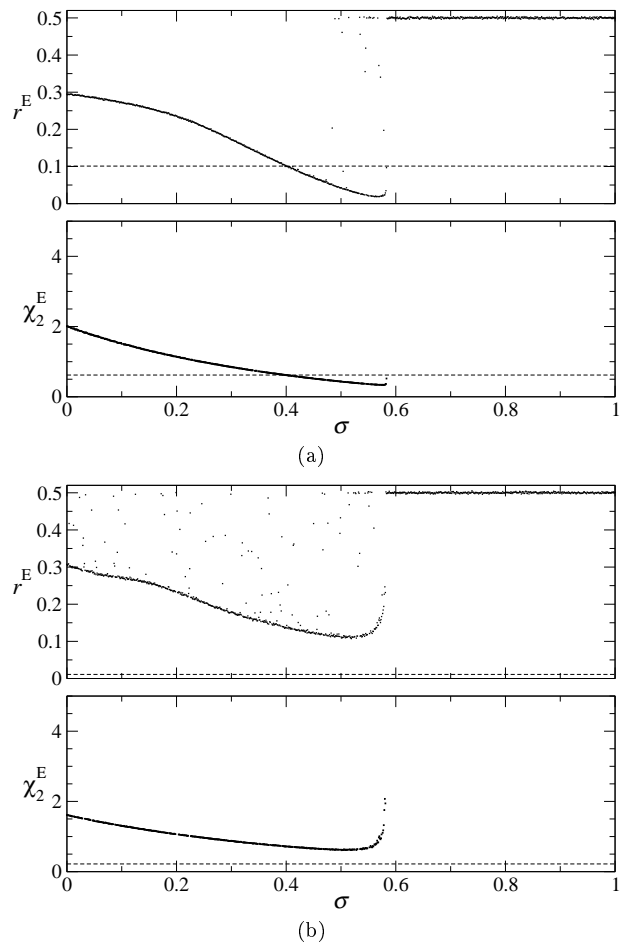


FIG. 24: Bit error rate r^E and response function χ_2^E as a function of σ , for Bernoulli map, $\tau = 50$, $\varepsilon = 0.8$ and Eqs. (2) and (45). The values for unit B (which are not dependent of σ) are shown as dashed lines. (a) $\kappa = 0.4$; (b) $\kappa = 0.75$

message by a mechanism which has been named *chaos pass filter*. Thus chaos pass filter is the linear response of a synchronized chaotic system to a quasi-random binary perturbation. This perturbation has a component which is acting transverse to the synchronization manifold. Hence the message drives the system away from synchronization whereas the dynamics of the system, quantified by conditional Lyapunov exponents, brings the trajectories back to the manifold. The competition between these two effects leads to the chaos pass filter which allows the receiving unit to recover the message by subtracting its own chaotic trajectory from the received signal.

Consequently, one expects that perturbations of the sender are just damped by the receiver; the receiver filters out the perturbation and responds essentially with the unperturbed trajectory. However, our numerical and analytical investigations of iterated maps show that the mechanism of chaos pass filter is much more complex. The response of the receiver to the perturbation of the sender can be very large. Close to the synchronization boundary it diverges. But even deep inside the region

of synchronization where the transverse Lyapunov exponents are negative and large, the receiver makes large excursions away from the synchronization manifold resulting in a power law and diverging moments of the distribution of deviations between the sending and receiving trajectory. Mathematically, this behavior is a consequence of multiplicative and additive noise appearing in the equations of linear response.

In addition, the linear response to a periodic perturbation shows resonances due to the delayed self-feedback of the sending unit. Depending on parameters and frequency, those resonances can be very large but the response can also be suppressed.

A message produces a broad distribution of deviations between the trajectories of sender and receiver. The bit error rate is given by an integral over this distribution. It turns out that the bit error rate approaches continuously the maximal value 50% at the synchronization boundary, as expected. But inside the region of synchronization the bit error rate shows a complex nonmonotonic behavior which cannot be related to the properties of transverse Lyapunov exponents.

In special cases we could calculate the bit error rate analytically. Relating it to an iterated function system we found a fractal distribution of deviations yielding a devil's staircase for the bit error rate as a function of model parameters.

Adding additional noise to the chaotic transmitted signals can reduce the bit error rate. This opens the possibility to improve the security of chaos communication with bi-directional transmission of chaotic signals. When the receiver adds an additional message or noise to its transmitted signal he can improve his bit error rate (*mutual chaos pass filter*).

With respect to secure communication, the difference between uni- and bi-directional couplings of the two partners has been investigated in detail. Assume that a third attacking unit has knowledge about all details of the chaotic systems and can record the transmitted signals. When the two partners are coupled uni-directionally, a third attacking unit can synchronize as well, and retrieve the secret message. However, when the two units are interacting by a bi-directional transmission of signals, an attacker may have problems to synchronize as well. It turns out that an attacker who can record and adjust both lines of transmission can synchronize. In this case even the mutual chaos pass filter does not help and one needs more advanced methods like secret commutative filters to establish a secure communication [17]. But when the attacker can only adjust to one direction of transmission, one can find parameters such that the bit error rate of the attacker is much larger than the one of the partners.

Acknowledgments

We would like to thank Georg Reents for helpful dis-

cussions.

APPENDIX A: ANALYTIC RESULTS FOR THE BIT ERROR RATE

Outside the synchronization region the bit error rate trivially equals $\frac{1}{2}$. Inside the synchronization region in general, the bit error rate has to be determined by means of computer simulations. However, for some special cases it can be calculated analytically.

1. Logistic map, uni-directional setup, $\tau = 1$, $\varepsilon = 1$, $\kappa = 0$

In the case of the uni-directional setup (case (a) of Fig. 1) with the logistic map and no delay ($\tau = 1$), the bit error rate can be calculated for the point $\varepsilon = 1$. The dynamics is given by

$$\begin{aligned} a_t &= f(a_{t-1}) \\ b_t &= f(a_{t-1} + m_{t-1}), \end{aligned} \quad (\text{A1})$$

from which follows that

$$d_t = f'_{t-1} m_{t-1}. \quad (\text{A2})$$

From the facts that (1) f'_{t-1} and m_{t-1} are uncorrelated, (2) the probability distribution of f' is symmetric about $f' = 0$ and (3) $m_t = \pm M$, follows that d has basically the same probability distribution as f' . Therefore, the bit error rate can easily be calculated, see Eqs. (26) and (11):

$$\begin{aligned} r &= \frac{1}{2} \left(1 - \int_{-M}^M p(d) dd \right) = \frac{1}{2} \left(1 - \int_{-1}^1 \rho(f') df' \right) \\ &= \frac{\text{arcsec}(4)}{\pi} \approx 0.4196. \end{aligned} \quad (\text{A3})$$

This is in agreement with the numerical simulations shown in Fig. 9

2. Logistic map, bi-directional setup, $\tau = 1$, $\varepsilon = \frac{1}{2}$, $\kappa = 0$

Similarly, in the bi-directional case, the bit error rate can be calculated for $\varepsilon = \frac{1}{2}$: The dynamics is given by

$$\begin{aligned} a_t &= \frac{1}{2} f(a_{t-1}) + \frac{1}{2} f(b_{t-1}) \\ b_t &= \frac{1}{2} f(b_{t-1}) + \frac{1}{2} f(a_{t-1} + m_{t-1}) \end{aligned} \quad (\text{A4})$$

from which follows that

$$d_t = \frac{1}{2} f'_{t-1} m_{t-1}. \quad (\text{A5})$$

Comparing this with Eq. (A2) leads to

$$r = \frac{1}{2} \left(1 - \int_{-2}^2 \rho(f') df' \right) = \frac{1}{3} \quad (\text{A6})$$

which is also in agreement with the numerical simulations shown in Fig. 9.

3. Bernoulli map, $\tau = 1$

In parts of Fig. 8 one can discover a staircase structure for the bit error rate. For the uni-directional setup this is true for $\varepsilon \geq \frac{2}{3}$, while for the bi-directional setup this is valid for $\frac{1}{3} \leq \varepsilon \leq \frac{2}{3}$. For these regions the bit error rate can be calculated analytically. If one takes a closer look at the staircases, Fig. 25, it becomes apparent that they have infinitely many steps, i.e. they are a kind of devil's staircase.

a. Uni-directional coupling

This staircase structure should be explained here for the case of uni-directional coupling. The equation for the distance can be written in the following way, see also Eq. (10):

$$d_t = \begin{cases} d_t^- = \frac{3}{2}(1-\varepsilon)d_{t-1} - \frac{3}{2}\varepsilon M \\ d_t^+ = \frac{3}{2}(1-\varepsilon)d_{t-1} + \frac{3}{2}\varepsilon M \end{cases} \quad (\text{A7})$$

The two equations represent the two different bits. If d_t is plotted versus d_{t-1} , then d_t^- and d_t^+ are two parallel straight lines, see Fig. 26. The values of this iteration $d_t(d_{t-1})$ generate the distribution $p(d)$ from which, in principle, the bit error rate can be calculated. The dashed boxes (--) in Fig. 26 represent the interval which d_t is bounded to (due to the attracting fixed points). For $\varepsilon < \frac{2}{3}$ the two maps d_t^- and d_t^+ have a certain overlap in their co-domain, see Fig. 26(a) (the co-domains are indicated by gray stripes). This fact makes the distribution $p(d)$ complicated. However, for $\varepsilon > \frac{2}{3}$ the two maps have no overlap, see Fig. 26(c), and the distribution is manageable analytically. As a result of the gap in the co-domain (indicated by a zigzag pattern), a gap in the domain emerges in the next time step. The latter gap produces two further gaps in the co-domain which become gaps in the domain in the next time step. The result of this iterative process is that the distribution $p(d)$ has a fractal support. The first and largest gaps are shown in Fig. 27. The first gap is called G . The gaps produced by G are G^- and G^+ . The gaps coming from G^+ are called G^{-+} and G^{++} ; the gaps coming from G^- are called G^{--} and G^{+-} and so on.

Now we want to calculate the exact position of the gaps. The fixed points of d^- and d^+ are called d_*^- and

d_*^+ . One can easily calculate that

$$d_*^- = -\frac{3\varepsilon M}{3\varepsilon - 1} \quad \text{and} \quad (\text{A8})$$

$$d_*^+ = +\frac{3\varepsilon M}{3\varepsilon - 1}. \quad (\text{A9})$$

From Fig. 26(c) it can be seen that

$$G =]d^-(d_*^+), d^+(d_*^-)[\\ =]-\frac{3\varepsilon(3\varepsilon - 2)M}{3\varepsilon - 1}, \frac{3\varepsilon(3\varepsilon - 2)M}{3\varepsilon - 1}[\quad (\text{A10})$$

which is about $]-0.19M, 0.19M[$ for $\varepsilon = 0.7$, see Fig. 27. The gap G^+ is generated by applying d^+ to G , i.e.

$$G^+ =]d^+(d^-(d_*^+)), d^+(d^+(d_*^-)))[\\ =]\frac{3\varepsilon(5 - 12\varepsilon + 9\varepsilon^2)M}{2(3\varepsilon - 1)}, -\frac{3\varepsilon(5 - 12\varepsilon + 9\varepsilon^2)M}{2(3\varepsilon - 1)}[\quad (\text{A11})$$

which is about $]0.96M, 1.14M[$ for $\varepsilon = 0.7$, see Fig. 27.

Then the gap G^{-+} , for example, is generated by applying d^- to G^+ , i.e.

$$G^{-+} =]d^-(d^+(d^-(d_*^+))), d^-(d^+(d^+(d_*^-)))][\quad (\text{A12})$$

and so on.

Due to the constant and equal slope of d^- and d^+ , and due to the fact that there is no overlap between the co-domains of d^- and d^+ , the relative frequency of all distances d which occur (i.e. which are not inside a gap) are equal. This means that Fig. 27 can also be seen as the corresponding histogram; all bars have the same height.

The bit error rate is related to the integral from $-M$ to $+M$ over the distribution of the distances, see Eq. (26). From Fig. 27 it can be seen that for $\varepsilon = 0.7$ this integral exactly equals $\frac{1}{2}$; thus, the bit error rate equals $\frac{1}{4}$, which is in agreement with Fig. 25.

If ε is changed, then the positions of the gaps are changed, too. As long as the gap G^+ contains the value $+M$ (= as long as the gap G^- contains the value $-M$), the integral yields $\frac{1}{2}$ and the bit error rate is $\frac{1}{4}$. This explains the plateau AB in Fig. 25. With the aid of Eq. (A11) we can calculate the exact position of this plateau:

$$\text{A: } \varepsilon = \frac{2}{3} = 0.\bar{6}, \quad (\text{A13})$$

$$\text{B: } \varepsilon = \frac{1}{3}(1 + \sqrt{2}) \approx 0.804738. \quad (\text{A14})$$

Similarly, one gets the point C of Fig. 25. The bit error rate becomes $\frac{1}{2}$ when the integral starts to be 0. This is when the gap G is as large as (or larger than) the interval $[-M, M]$. Considering Eq. (A10) yields:

$$\text{C: } \varepsilon = \frac{1}{6}(3 + \sqrt{5}) \approx 0.872678. \quad (\text{A15})$$

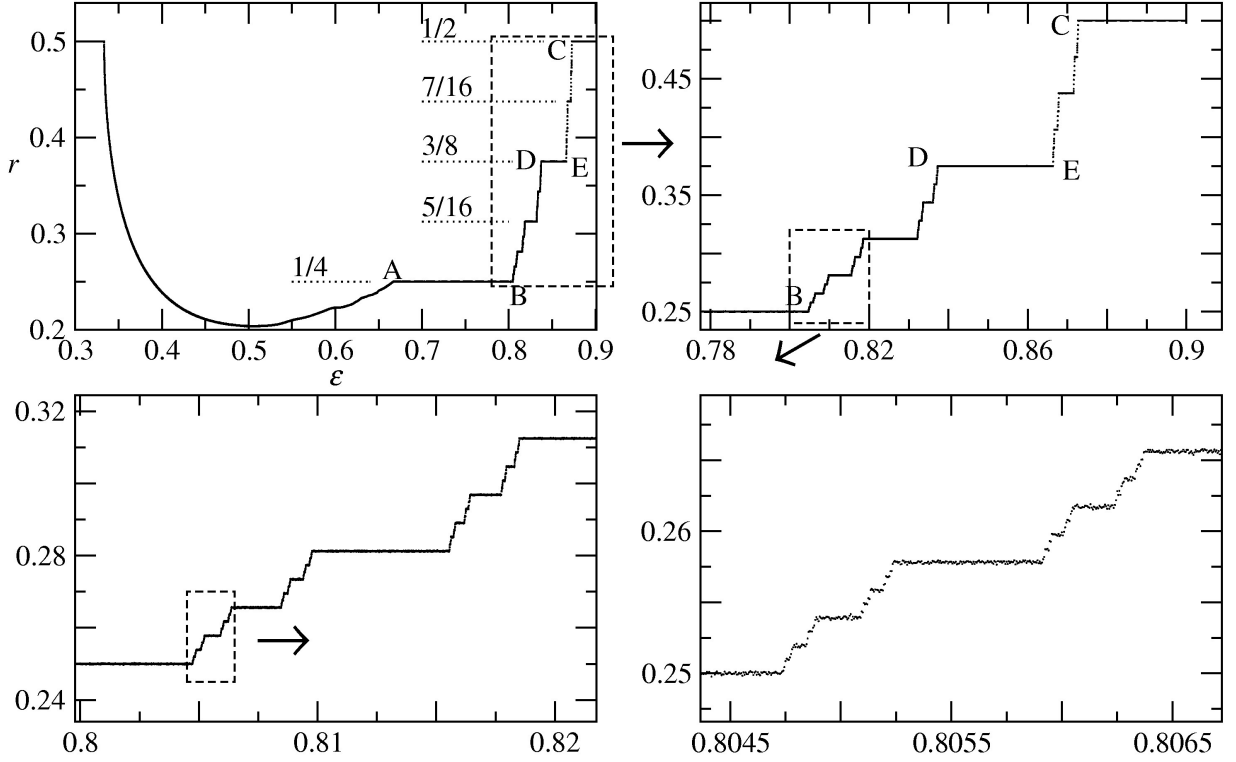


FIG. 25: Bit error rate r for Bernoulli map, $\tau = 1$, $\kappa = 0$, uni-directional coupling, see also Fig. 8. Zooming in the staircase structure reveals more and more steps.

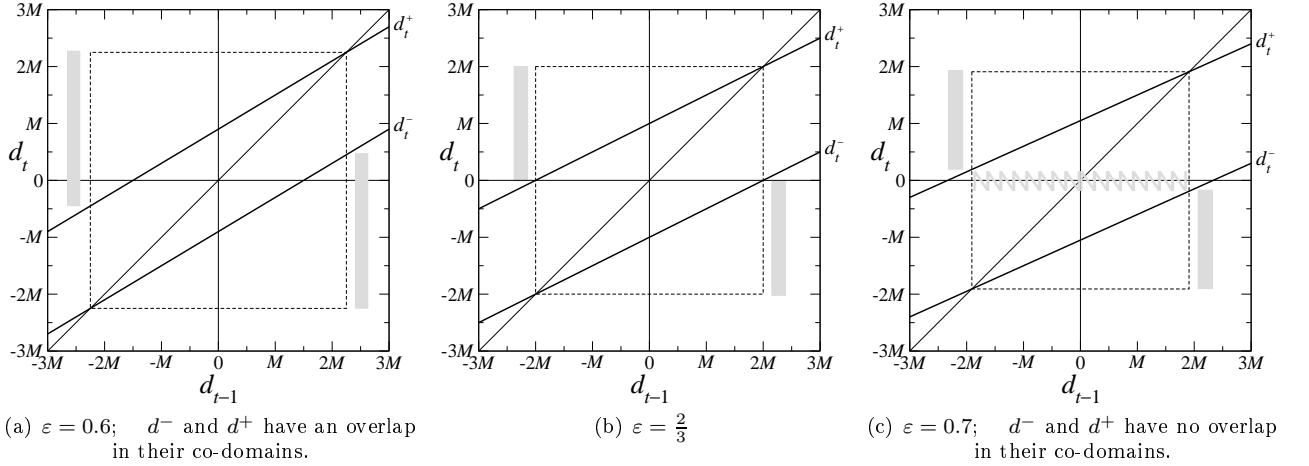


FIG. 26: The iteration $d_t(d_{t-1}) = d_t^\pm(d_{t-1})$ of the distances for different coupling parameters ε . The dashed boxes represent the interval which d is bounded to due to the fixed points. Additionally, the bisecting line $d_t(d_{t-1}) = d_{t-1}$ is plotted. The gray stripes show the co-domains of d^- and d^+ .

The plateau DE, which has the value $\frac{3}{8}$, can be calculated considering the gap G^{+-} . One gets:

$$D: \varepsilon \approx 0.837266 \quad (\text{A16})$$

$$E: \varepsilon \approx 0.866386 \quad (\text{A17})$$

All other plateaus can be calculated with the aid of smaller gaps.

b. Bi-directional coupling

The calculations for the case of bi-directional coupling are very similar to the ones for the uni-directional case. Here, only few results should be shown.

For

$$0.\bar{3} = \frac{1}{3} \leq \varepsilon \leq \frac{5}{9} = 0.\bar{5} \quad (\text{A18})$$

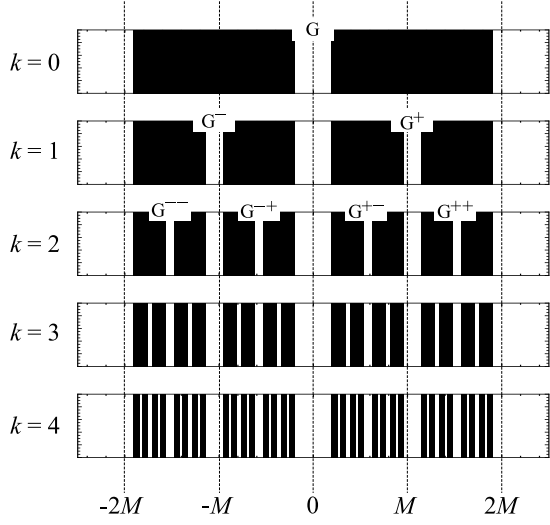


FIG. 27: Gaps in the domain/co-domain/distribution of d^- and d^+ for different recursion depths k . $\varepsilon = 0.7$.

the bit error rate is 0.

For

$$0.5749 \approx \frac{1}{6} + \frac{1}{\sqrt{6}} \leq \varepsilon \leq \frac{2}{3} = 0.\bar{6} \quad (\text{A19})$$

the bit error rate is $\frac{1}{4}$.

APPENDIX B: NOISE-REDUCED BIT ERROR RATE

The integral of Eq. (32) can be calculated if the noise has a flat distribution in the interval $w \in [-W, W]$ with $p_w(w) = \frac{1}{2W}$. The problem can be split up into three intervals.

- $W < \frac{M}{2}$

$$r^B = \frac{1}{2\pi W} \int_{-W}^W \sec^{-1} \left(2 + \frac{2w}{M} \right) dw \quad (\text{B1})$$

- $\frac{M}{2} < W < \frac{3}{2}M$

$$r^B = \frac{1}{2\pi W} \int_{-M/2}^W \sec^{-1} \left(2 + \frac{2w}{M} \right) dw \quad (\text{B2})$$

- $W > \frac{3}{2}M$

$$r^B = \frac{1}{2\pi W} \left(\int_{-M/2}^W + \int_{-M/2}^{W-2M} \right) \sec^{-1} \left(2 + \frac{2w}{M} \right) dw \quad (\text{B3})$$

The result is:

- $W < \frac{M}{2}$

$$r^B = g(W) - g(-W) \quad (\text{B4})$$

- $\frac{M}{2} < W < \frac{3}{2}M$

$$r^B = g(W) \quad (\text{B5})$$

- $W > \frac{3}{2}M$

$$r^B = g(W) + g(W - 2M) \quad (\text{B6})$$

with

$$g(w) = \frac{1}{2\pi W} \left\{ (M + w) \sec^{-1} \left(2 + \frac{2w}{M} \right) - \frac{M}{2} \ln \left[\left(2 + \frac{2w}{M} \right) + \sqrt{\left(2 + \frac{2w}{M} \right)^2 - 1} \right] \right\} \quad (\text{B7})$$

-
- [1] L. M. Pecora and T. L. Carroll, Phys. Rev. Lett. **64**, 821 (1990).
- [2] A. Pikovsky, M. Rosenblum, and J. Kurths, *Synchronization, a universal concept in nonlinear sciences* (Cambridge University Press, Cambridge, 2001).
- [3] H. G. Schuster and W. Just, *Deterministic Chaos* (Wiley VCH, Weinheim, 2005).
- [4] E. Klein, N. Gross, M. Rosenbluh, W. Kinzel, L. Khaykovich, and I. Kanter, Phys. Rev. E **73**, 066214 (2006).
- [5] I. Fischer, R. Vicente, J. M. Buldu, M. Peil, C. R. Mirasso, M. C. Torrent, and J. García-Ojalvo, Phys. Rev. Lett. **97**, 123902 (2006).
- [6] S. Sivaprakasam, J. Paul, P. S. Spencer, P. Rees, and K. A. Shore, Opt. Lett. **28**, 1397 (2003).
- [7] M. W. Lee, J. Paul, C. Masoller, and K. A. Shore, J. Opt. Soc. Am. B **23**, 846 (2006).
- [8] K. M. Cuomo and A. V. Oppenheim, Phys. Rev. Lett. **71**, 65 (1993).
- [9] L. Kocarev and U. Parlitz, Phys. Rev. Lett. **74**, 5028 (1995).
- [10] G. D. VanWiggeren and R. Roy, Science **279**, 1198 (1998).
- [11] W. Kinzel and I. Kanter, in *Handbook of Chaos Control*, edited by E. Schöll and H. Schuster (Wiley-VCH, Weinheim, 2008), 2nd ed.
- [12] A. Argyris, D. Syvridis, L. Larger, V. Annovazzi-Lodi, P. Colet, I. Fischer, J. García-Ojalvo, C. R. Mirasso, L. Pesquera, and K. A. Shore, Nature **438**, 343 (2005).
- [13] A. Murakami and K. A. Shore, Phys. Rev. A **72**, 053810 (2005).
- [14] I. Fischer, Y. Liu, and P. Davis, Phys. Rev. A **62**, 011801 (2000).
- [15] E. Klein, R. Mislovaty, I. Kanter, and W. Kinzel, Phys. Rev. E **72**, 016214 (2005).
- [16] E. Klein, N. Gross, E. Kopelowitz, M. Rosenbluh, L. Khaykovich, W. Kinzel, and I. Kanter, Phys. Rev. E **74**, 046201 (2006).
- [17] I. Kanter, E. Kopelowitz, J. Kestler, and W. Kinzel, *Chaos synchronization with dynamic filters: two way is better than one way*, to be published.
- [18] B. Cessac and J.-A. Sepulchre, Physica D **225**, 13 (2007).
- [19] H. Nakao, Phys. Rev. E **58**, 1591 (1998).
- [20] M. Rosenbluh, Y. Aviad, E. Cohen, L. Khaykovich, W. Kinzel, E. Kopelowitz, P. Yoskovits, and I. Kanter, Phys. Rev. E **76**, 046207 (2007).
- [21] I. Kanter, N. Gross, E. Klein, E. Kopelowitz, P. Yoskovits, L. Khaykovich, W. Kinzel, and M. Rosenbluh, Phys. Rev. Lett. **98**, 154101 (2007).
- [22] J. Kestler, W. Kinzel, and I. Kanter, Phys. Rev. E **76**, 035202 (2007).
- [23] J. Kestler, E. Kopelowitz, I. Kanter, and W. Kinzel, Phys. Rev. E **77**, 046209 (2008).
- [24] D. Sornette, Phys. Rev. E **57**, 4811 (1998).
- [25] Y. Kuramoto and H. Nakao, Phys. Rev. Lett. **78**, 4039 (1997).
- [26] L. Ein-Dor and I. Kanter, Phys. Rev. E **60**, 799 (1999).
- [27] M. Barnsley, *Fractals Everywhere* (Academic Press, San Diego, 1988).
- [28] M. Mützel, *Diploma thesis: Chaos-Filter bei chaotischen Abbildungen mit zeitlicher Verzögerung* (University of Würzburg, 2007).
- [29] T. Heil, I. Fischer, W. Elsässer, J. Mulet, and C. R. Mirasso, Phys. Rev. Lett. **86**, 795 (2001).